Eur. Phys. J. A **30**, 165–182 (2006)
DOI 10.1140/epja/i2006-10114-9

THE EUROPEAN PHYSICAL JOURNAL A

Isotopic compositions and scalings

M. Colonna[1,a] and M.B. Tsang[2]

[1] Laboratori Nazionali del Sud INFN via S. Sofia 62 and Dipartimento di Fisica e Astronomia, Universitá di Catania, I-95123 Catania, Italy
[2] National Superconducting Cyclotron Laboratory, Michigan State University, East Lansing, MI 48824, USA

Received: 2 March 2006 /
Published online: 23 October 2006 –

Abstract. We review experimental and theoretical studies devoted to extract information on the behaviour of the symmetry energy, in density regions different from the normal value, with charge-asymmetric reactions at Fermi energies. In particular, we focus on the analysis of fragmentation reactions and isotopic properties of the reaction products. Results concerning "isoscaling" properties and the N/Z equilibration among the reaction partners in semi-peripheral reactions are also discussed.

PACS. 21.30.Fe Forces in hadronic systems and effective interactions – 25.70.-z Low and intermediate energy heavy-ion reactions – 25.70.Lm Strongly damped collisions – 25.70.Pq Multifragment emission and correlations

1 Introduction

Heavy-ion collisions at Fermi energies offer the possibility to learn about the nuclear effective interaction in regions where the density and temperature are different from those of the stable nuclei. In particular, in charge-asymmetric systems, one can access information on the behaviour of the symmetry energy, E_{sym}, that is poorly known at low and high densities. Not only is the symmetry energy relevant for structure properties, being linked to the thickness of the neutron skin in heavy nuclei (see [1]), but this information is of interest also in the astrophysical context, providing constraints to the equation of state used in astrosphysical calculations [2,3]. Such information is essential for the understanding of the properties of supernovae and neutron stars [4–9].

In fig. 1 (bottom panel) we show the density dependence of the potential symmetry energy contribution, $E_{sym,pot}$ for three different effective interactions. While all curves cross around normal nuclear-matter density ρ_0, there are large differences, particularly in high-density regions. Even at the relatively well-known "crossing point" at normal density, various effective forces give controversial predictions for the momentum dependence of the fields acting on the nucleons and, consequently, for the splitting of the neutron/proton effective masses, which are important in nuclear structure and nuclear reaction dynamics. For discussion purpose, we will call interactions such as BPAL32 asy-stiff and such as SKM* asy-soft (fig. 1, ref. [10]).

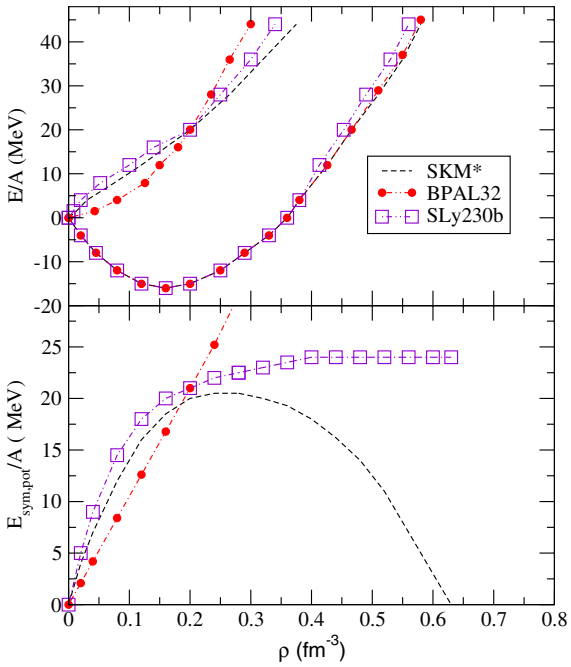

Fig. 1. Equation of state (EOS) for various effective forces. Top: neutron matter (upper curves), symmetric matter (lower curves). Bottom: potential symmetry energy. From [10].

Fragmentation mechanisms at Fermi energies can be used to study the symmetry energy at densities below and around the normal value. In violent collisions, where the full disassembly of the system into many fragments is ob-

[a] e-mail: colonna@lns.infn.it

served, one can study new properties of liquid-gas phase transitions occurring in asymmetric matter. In neutron-rich matter, phase co-existence leads to different asymmetries in the liquid and in the gas phase: fragments (liquid) appear more symmetric with respect to the initial system, while light particles (gas) are more neutron rich [11–15]. This effect, caused by the decrease in the symmetry energy when the density gets lower, can be used to investigate the behaviour of the derivative of the symmetry energy with respect to density. The width of the isotopic distributions is more connected to the value of the symmetry energy. Information on the low-density properties of the symmetry energy can be obtained from fragmentation studies. Similarly, complementary information is obtained from the study of emitted nucleons and light particles (pre-equilibrium phase). The importance of the isotopic degree of freedom to obtain information about charge equilibration and its relation to the charge asymmetry dependent terms of the EOS has been recently pointed out [16]. We will review here experimental and theoretical results about isotopic properties of reaction products, with the aim of extracting information about the behaviour of the symmetry energy. The paper is organized as follows: we will first review results concerning the properties of pre-equilibrium emission and fragment isotopic content, iso-distillation, then we will discuss the relation of fragment isotopic distributions to the symmetry energy behaviour, focusing, in particular, on the recently introduced isoscaling analysis. Finally, we will discuss isospin transport mechanisms in mid-peripheral reactions and N/Z equilibration, before concluding.

2 Isospin effects on pre-equilibrium emission

Heavy-ion reactions, at energies larger than 30 MeV/A, are characterized by pre-equilibrium emission, fast particles emitted before and during thermalization, see ref. [17] and references therein. For nuclear collisions around the Fermi energy, fast particles are emitted mostly during the expansion phase, when the composite system has reached a density below normal making it possible to extract information on the behaviour of the symmetry energy at sub-normal densities. In collisions between neutron-rich nuclei, the N/Z of the pre-equilibrium emission directly reflect the value of the symmetry energy (being larger for larger values of E_{sym}). In dynamical models such as those based on the Boltzmann-Nordheim-Vlasov equations (BNV) or the Boltzmann-Uehling-Uhlenbeck approach (BUU) as well as stochastic mean-field (SMF) simulations, one observes different N/Z composition of pre-equilibrium emission depending on the asymmetric part of the nuclear equation of state (asy-EOS). At low density, the symmetry energy is larger in the asy-soft case, favoring neutron emission, than in the asy-stiff case. Similar results are obtained by molecular-dynamics studies, as discussed below [18,19].

We will define emitted particles in the "gas phase" as those particles localized in low-density regions ($\rho < \rho_0/3$ for instance), while the remaining matter will be identified as "liquid phase". Pre-equilibrium emission can be associated with particles emitted (gas phase) at the first collisional stage, *i.e.* up to $\approx$ 100–150 fm/c. Obviously, the properties of the "liquid phase" will be influenced by the characteristics of this particle emission. Figure 2 shows the time evolution of $(N/Z)_{gas}$ (left panel) and $(N/Z)_{liq}$ (right panel) for the reaction $^{124}\mathrm{Sn} + ^{124}\mathrm{Sn}$ at 50 MeV/A, $b = 2$ fm, obtained with the isospin quantum molecular dynamics (IQMD) model considering the full nucleon-nucleon interaction (full line), with Coulomb potential only (dashed line) and with symmetry potential only (dotted line). An asy-stiff parameterization has been used for the symmetry energy. The Coulomb interaction reduces the N/Z of the pre-equilibrium emission, while the symmetry energy enhances it. At $t \approx 150$ fm/c one obtains $(N/Z)_{gas} \approx 1.5$ while $(N/Z)_{liq} \approx 1.4$. Hence the gas phase is more neutron rich.

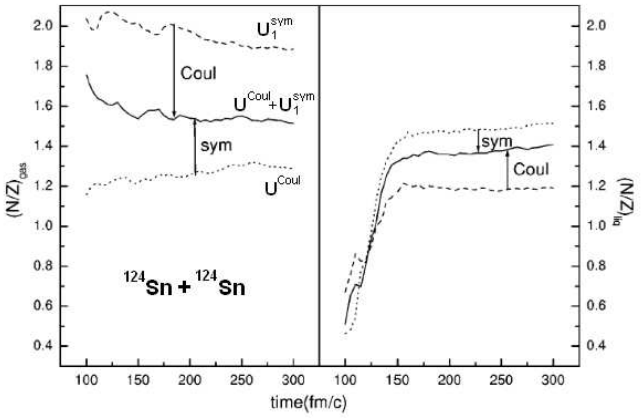

Fig. 2. The time evolution of $(N/Z)_{gas}$ (left panel) and $(N/Z)_{liq}$ (right panel) for three combinations of Coulomb and symmetry interactions, for the reaction $^{124}\mathrm{Sn} + ^{124}\mathrm{Sn}$ at 50 MeV/A and impact parameter $b = 2$ fm, as obtained in IQMD.

It is worthwhile to compare results obtained with the different transport models quantitatively. In ref. [20], the same reaction has been studied with the BUU code. Values of the $(N/Z)_{liq} = 1.44$ are obtained at $t = 100$ fm/c with an asy-stiff parameterization while an asy-soft parameterization leads to $(N/Z)_{liq} = 1.23$. The value compares rather well (within 3%) with the results of the IQMD model. The different time scales in the two models depend on the definition of the "liquid phase", that for IQMD corresponds to cluster and intermediate mass fragment (IMF) emission, while in the BUU model it is associated with a composite excited source. As shown in fig. 3, these results are also in agreement with stochastic mean-field (SMF) simulations. Indeed, one observes that, with an asy-stiff parameterization of the symmetry energy, after around 100 fm/c, the asymmetry $I = (N - Z)/A$ of the liquid phase equals 0.18, corresponding to $(N/Z)_{liq} = 1.44$.

The antisymmetrized molecular dynamics (AMD) simulations for different Ca isotopes at 35 MeV/A are studied in ref. [18]. For the $^{48}\mathrm{Ca} + ^{48}\mathrm{Ca}$ reaction, that has roughly

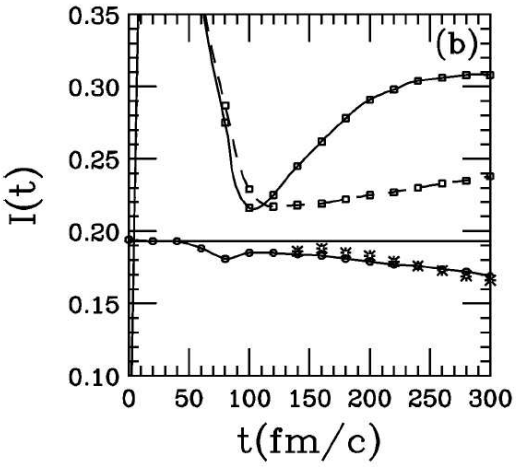

Fig. 3. Time evolution of the asymmetry of the liquid phase (circles, lower curve), gas phase (squares, dashed line) and gas phase in a central region (squares, full line), for the reaction ^{124}Sn + ^{124}Sn at 50 MeV/A, $b = 2$ fm, SMF calculations. An asy-stiff parameterization of the symmetry energy has been used.

the same asymmetry of the ^{124}Sn + ^{124}Sn reaction, one observes that after $\approx 80\,\mathrm{fm}/c$, $(Z/A)_{liq} = 0.42$ corresponding to $(N/Z)_{liq} = 1.39$ (using an asy-stiff equation of state, Gogny-AS). However, at later times, $t \approx 300\,\mathrm{fm}/c$, the liquid phase appears to be more symmetric in the BUU calculations [18]. This indicates that the rate of neutron enrichment of the gas phase is not the same and may be related to the different evolution of the system in the two models. Indeed AMD calculations include clusters in the disassembly of the excited system, while in BUU calculations only a composite single excited source, that emits nucleons, not clusters, survives until late times. The isospin content of fragments formed in dissipative collisions at intermediate energies will be discussed in the next section.

It is interesting to look at the behaviour of pre-equilibrium emission in reactions at higher beam energies [21–23]. In this case, particles are emitted mostly from the high-density region (compression phase), allowing one to test the behaviour of the symmetry energy at densities above saturation. Pre-equilibrium emission is also sensitive to the momentum dependence of the isospin-dependent (iso-vector) part of the nuclear interaction. Typical BUU calculations are shown in fig. 4 for the reaction ^{132}Sn + ^{124}Sn at 400 MeV/A. The figure shows rapidity distributions of pre-equilibrium neutrons and protons, at $b = 5$ fm obtained with four interactions formed from the combinations of with (MDI) or without (MDYI) momentum dependence in the iso-vector part of the nuclear interaction with asy-soft (1) or asy-stiff (0) parameterizations of the density behaviour of the symmetry energy. With an asy-stiff parameterization (thick dashed and solid lines) more neutrons are emitted compared to the corresponding asy-soft parameterization (grey dashed and dotted line). This trend is the opposite to the low-density region as the symmetry energy for the asy-stiff parameterization is higher in

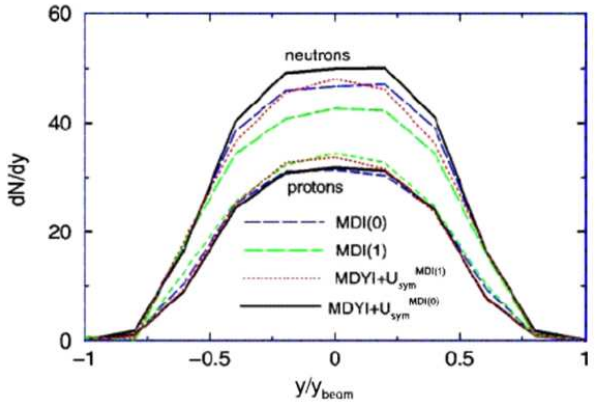

Fig. 4. Rapidity distributions of neutrons and protons, obtained in the reaction ^{132}Sn + ^{124}Sn at 400 MeV/A, $b = 5$ fm. The results of four interactions are presented: the MDI(0), asy-stiff (thick dashed line) and MDI(1), asy-soft (grey dashed line), that contain momentum dependence also in the isovector part of the interaction; the MDYI(0) (thick solid line) and MDYI(1) (dotted line), that are without iso-momentum dependence. From [21].

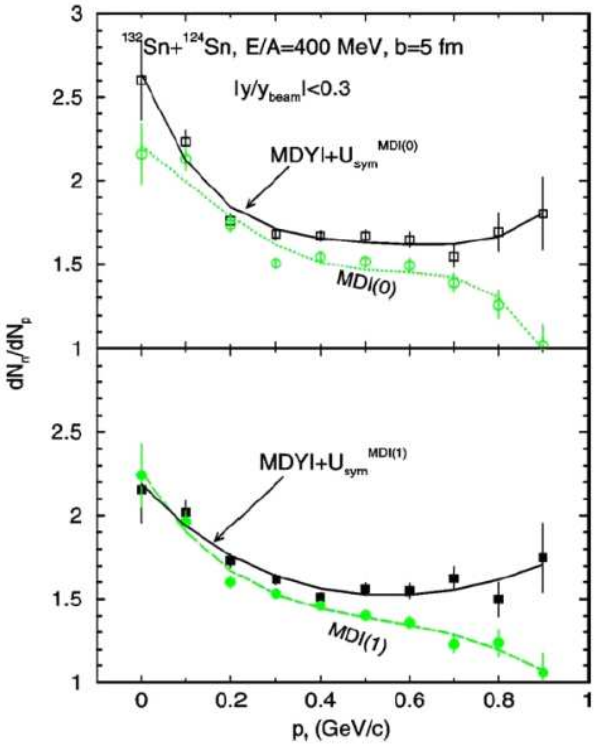

Fig. 5. Neutron to proton ratio, as a function of transverse momentum, for the same reaction and interactions of fig. 4. From [21].

the high-density phase. However, when the momentum dependence is implemented, less neutrons are emitted (compare the thick full line and grey dashed lines for instance). Indeed, for the interactions considered here, a splitting of neutron and proton effective masses with $m^*_n > m^*_p$ is obtained. This reduces the neutron repulsion. Therefore, we observe a kind of compensation between the effects due to

the density dependence and to the momentum dependence of the symmetry potential. In fact, the thick dashed line (asy-stiff interaction with momentum dependence) and the dotted line (asy-soft interaction without momentum dependence) almost overlap. On the other hand, if the interactions have the opposite splitting, $m_n^* < m_p^*$, neutrons would be more repelled [22,24]. In fig. 5 the neutron to proton ratio is plotted as a function of transverse momentum, for particles in the mid-rapidity region. It is clear that the decrease of N/Z observed with the MDI interactions (see fig. 4) can be attributed to the high-momentum tail of the nucleon emission that is more sensitive to the momentum dependence.

In summary, the study of pre-equilibrium emission, as a function of the beam energy, can be considered as an interesting and promising tool to explore the reaction dynamics and to investigate the behaviour of the symmetry energy from low to high density. The isotopic composition, N/Z, of all emitted particles appears to be sensitive to the stiffness of the symmetry energy while the dependence of the isotopic content on rapidity, or transverse momentum, appears to be a good candidate to study the momentum dependence of the isovector part of the nuclear interaction.

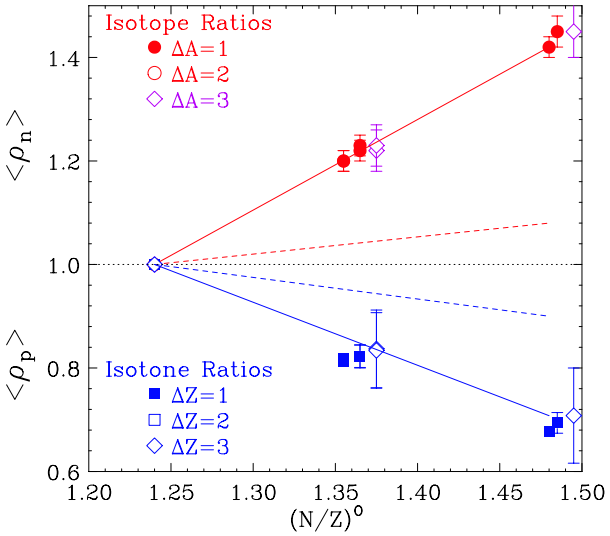

Fig. 6. The mean relative free neutron and free proton density as a function of $(N/Z)_0$. The dashed lines are the expected n-enrichment and p-depletion with the increase of isospin of the initial systems. The solid lines are drawn to guide the eye. From [30].

3 Isotopic composition of fragments: the iso-distillation

As a consequence of the initial collisional shock, or thermal expansion effects, the excited nuclear system expands and enters the low-density (co-existence) region of the nuclear-matter phase diagram. Here a phase separation occurs and fragments are formed, surrounded by a neutron-rich gas. This process is often referred to as isospin distillation or fractionation [14,25]. The isotopic composition of nuclear-reaction products provides important information on the reaction dynamics and the possible occurrence of a phase transition in asymmetric nuclear matter [10–12], which leads to separation into a symmetric dense phase (fragments) and an asymmetric dilute phase (nucleons and light particles) [10,12,25]. Such a phase transition can be generated by fluctuations of density or concentration, leading to a coupling of different instability modes. This mechanism is predicted, for instance, by stochastic mean-field (SMF) simulations [26], where fragments are formed due to the development of spinodal (volume) instabilities. After the first stage of particle emission, the asymmetry of the liquid phase still decreases (fig. 3) while fragments are being formed. Thus fragmentation is accompanied by the iso-distillation process. The amplitude of the effect is strictly related to the derivative of the symmetry energy, as we will discuss more in detail in the section devoted to isospin transport, while the width of the isotopic distributions is more connected to the symmetry energy value. The distillation effect is also predicted by statistical multifragmentation models [27–29], where the partition of the system into fragments and light particles is determined according to the statistical weights, that depend on the cluster (free) energies and hence also on the symmetry energy coefficient.

An experimental analysis of the N/Z of reaction products provides complementary information about the low-density dependence of the symmetry energy.

3.1 Experimental evidence

The N/Z degree of freedom has been studied experimentally with multifragmentation reactions [16,30,31]. Isotopically resolved data in the region $Z = 2$–8 have revealed systematic trends, which however are substantially affected by the decay of primary fragments.

In the study of the central collisions of four Sn systems at incident energy of 50 MeV per nucleon, the relative neutron and proton densities have been measured for the $^{112}\mathrm{Sn} + {}^{124}\mathrm{Sn}$, $^{124}\mathrm{Sn} + {}^{112}\mathrm{Sn}$, $^{124}\mathrm{Sn} + {}^{124}\mathrm{Sn}$, with respect to the $^{112}\mathrm{Sn} + {}^{112}\mathrm{Sn}$ system [30]. The extracted relative neutron (ρ_n) and proton (ρ_p) densities are shown in fig. 6; ρ_n increases while ρ_p decreases with the $(N/Z)_0$ ratio of the total system. The increase of ρ_n is consistent with neutron enrichment in the gas phase while the decrease of ρ_p suggests proton depletion. The experimental trend (data points with the solid lines drawn to guide the eye) is much stronger than the trend expected if neutrons and protons were homogeneously mixed (dashed lines) in the breakup configuration. Adopting an equilibrium breakup model, the observation is consistent with isospin fractionation, a signal predicted in the liquid-gas phase transition. Since the isospin fractionation is governed by the symmetry energy of the neutron and proton, it is a more general property of heavy-ion reactions than the liquid-gas phase phenomenon. In fact, dynamical models also give predictions of isospin amplification, in qualitative agreement with the data [30]. In this analysis, complete cancelation of the sequential effects is not necessary as long as

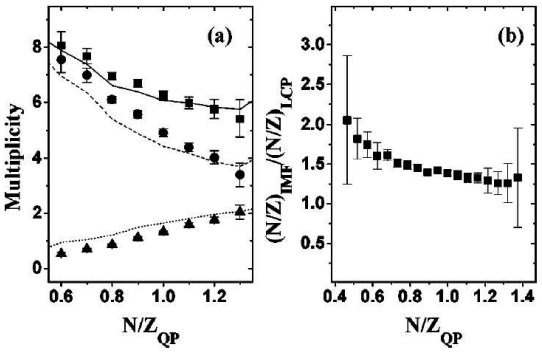

Fig. 7. a) Multiplicity of all charged particles (squares) as a function of the $(N/Z)_{QP}$ of the emitting PLF source, obtained in the reaction ^{28}Si + ^{112}Sn at 50 MeV/A. Circles and triangles represent the multiplicity of LCPs and IMFs, respectively. The lines are the results of model calculations. b) The ratio between the N/Z of IMFs and LCPs is plotted as a function of the $(N/Z)_{QP}$. From [32].

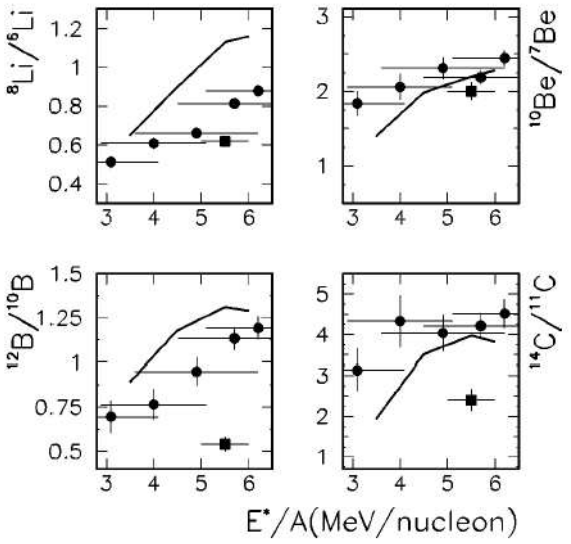

Fig. 8. Ratios of relative yields of neutron-rich to neutron-deficient isotopes, as a function of the excitation energy, as obtained in the fragmentation of PLF sources, from Au + Au at 35 AMeV (circles) or in central Xe + Cu collisions at 30 AMeV (squares). The lines are the predictions of SMM calculations. From [37].

the final yield is related to the primary fragment yield by a multiplicative factor [30].

The composition of intermediate mass fragments in several combinations of isospin asymmetry and excitation energy of the fragmenting source has been studied by considering quasi-projectiles created via peripheral reactions of ^{28}Si + ^{112}Sn and ^{124}Sn at 30 and 50 MeV/A [32]. The quasi-projectiles have been reconstructed from isotopically identified fragments. It is observed that the dependence of the mean fragment multiplicity and the mean N/Z ratio of the fragments on the $(N/Z)_{QP}$ ratio of quasi-projectiles are different for light charged particles (LCPs) and intermediate mass fragments (IMFs). This is illustrated in fig. 7, for the reaction ^{28}Si + ^{112}Sn at 50 MeV/A. The squares represent the multiplicity of all charged particles. This is then broken down into the multiplicity of light charged particles (circles) and the multiplicity of intermediate mass fragments (triangles). We can see that the IMF multiplicity increases with the $(N/Z)_{QP}$ of the system. The lines represent the results of hybrid calculations, obtained by combining a description of transfer processes in deep-inelastic reactions (DIT model, [33]) to statistical calculations of fragment production (statistical multifragmentation model, SMM). They are in good agreement with the data. In [20,30], the multiplicity of IMFs increases as a function of the multiplicity of charged particles for the more neutron-rich systems. However, the decrease in multiplicity of LCPs for neutron-rich systems in fig. 7 is not observed in the multifragmentation of the Sn + Sn system [34].

This effect, however, weakens at higher energies [35]. This is consistent with the temperature dependence of the isospin distillation effect predicted by the lattice-gas model [36] or by dynamical calculations [26]. The ratio $(N/Z)_{IMF}/(N/Z)_{LCP}$ decreases as $(N/Z)_{QP}$ increases, as shown in fig. 7(b). As there are fewer neutrons available, the excess protons go into the smaller fragments rather than the larger ones. Neutron-poor quasi-projectiles prefer to break up into very neutron-deficient (proton rich) LCPs and much more symmetric IMFs. On the contrary, neutron-rich quasi-projectiles break up into neutron-rich LCPs and more symmetric IMFs as a result of the distillation effect discussed before [12,14,25].

As for the evolution of the N/Z of fragments with the excitation energy of the fragmenting source, this is found to increase, as shown in ref. [37] for fragments emitted from excited PLF sources (see fig. 8). From the statistical point of view, this can be explained in terms of the larger amount of excitation energy available, that allows production of more exotic systems in a larger phase space. This effect is also compatible with the weakening of the distillation mechanism at high temperature, as discussed above.

4 Isoscaling in nuclear reactions

The availability of fragmentation data, obtained with good isotopic resolution for charge-asymmetric systems, makes it possible to examine systematic trends exhibited by isospin-dependent observables. In a series of recent papers, the scaling properties of cross-sections for fragment production with respect to the isotopic composition of the emitting systems were investigated [30,31]. The studied reactions include symmetric heavy-ion reactions at intermediate energy, leading to multifragment emission, as well as asymmetric reactions induced by α particles and ^{16}O projectiles at low to intermediate energies with fragment emission from excited heavy residues. To quantify the comparison of the isotope yields $Y(N,Z)$ obtained in reactions with different isospin asymmetry, the ratio $R_{21} = Y_2(N,Z)/Y_1(N,Z)$ is used. By convention, 2 denotes the more neutron-rich system.

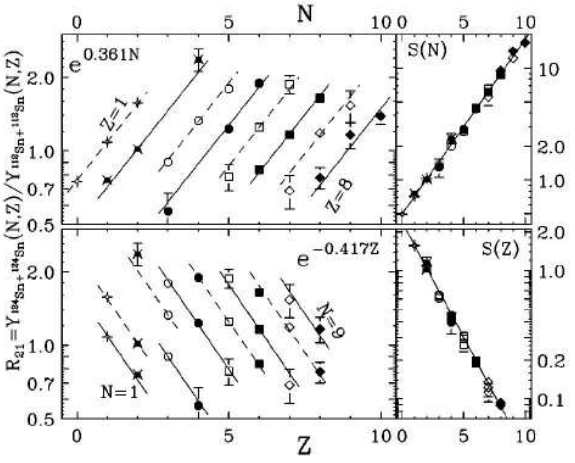

Fig. 9. The yield ratio R_{21} is plotted as a function of N (upper panel) or Z (lower panel). The central reactions considered are ^{124}Sn + ^{124}Sn and ^{112}Sn + ^{112}Sn at 50 MeV/A. From [38].

Figure 9 shows the isotope ratios, $R_{21}(N,Z)$, plotted as a function of N (upper panel) and Z (lower panel), for the central collisions of ^{124}Sn + ^{124}Sn and ^{112}Sn + ^{112}Sn, at 50 MeV/A. $R_{21}(N,Z)$ clearly exhibits an exponential dependence on N and Z, which is called the isoscaling relationship:

$$R_{21}(N,Z) = Y_2(N,Z)/Y_1(N,Z) = C \cdot \exp(N \cdot \alpha + Z \cdot \beta), \quad (1)$$

where C, α and β are fitting parameters. Since the introduction of isoscaling as an isospin observable, isoscaling has proved to be very robust and has been observed in many different types of reactions, such as multifragmentation, light ion-induced fragmentation, evaporation and deep-inelastic reactions [30,31,39,40]. There are also reports on the observation of isoscaling in spallation reactions [41] and, more recently, in fission [42], though the quality of the data is quite poor. Recent studies with realistic fission models [43] suggest that the behaviour of the isoscaling observed in fission is not the same as those observed in multifragmentation, *e.g.* the neutron isoscaling parameter α varies with the Z of the fission products. The most important aspect of isoscaling is its connection to symmetry energy and the temperature of the system, as will be discussed below.

4.1 Isoscaling in statistical models

Isoscaling arises very naturally within a statistical description of fragment production; it is the difference of the chemical potentials of systems with different (N_0/Z_0) ratio. In the grand-canonical statistical description of multifragmentation, the mean multiplicity of a fragment with mass number A and charge Z is given by

$$\langle N(A,Z)\rangle = g_{AZ}\frac{V_f}{\lambda_T^3}A^{3/2}\exp\Big[-\frac{1}{T}(F_{AZ}(T,\rho) - \mu_n(A-Z) - \mu_p Z)\Big], \quad (2)$$

where T is the temperature of the fragmenting source, g_{AZ} is the degeneracy factor of the fragment, λ_T is the nucleon thermal wavelength, V_f is the "free" volume, F_{AZ} is the fragment free energy and μ_n and μ_p are the neutron and proton chemical potentials, respectively. It follows immediately that, for two systems 1 and 2 with different total mass and charge but with the same temperature and density, the ratio of fragment yields is given by eq. (1) with parameters $\alpha = \Delta\mu_n/T$ and $\beta = \Delta\mu_p/T$.

In ref. [44], the chemical potentials for ^{124}Sn and ^{112}Sn are calculated with the grand-canonical version of the statistical multifragmentation model. Despite a considerable variation of the individual potentials, their difference $\Delta\mu = \mu_{112} - \mu_{124}$ changes only slightly as a function of the temperature. At $T > 5$ MeV, the results are similar to that obtained with the Markov chain version of the statistical multifragmentation model (SMM), which takes a completely microcanonical approach. At lower temperature different results are obtained indicating that the exact conservation of charge, mass and energy makes important differences whether the grand-canonical or microcanonical approximation is adopted. Calculating the difference of chemical potentials within the grand-canonical approximation, it is possible to connect the isoscaling parameter α to the difference of asymmetry (Z/A) between the two systems considered and the values of symmetry energy and temperature, through the relation

$$\xi = \alpha/(4\Delta(Z/A)^2) = C_{sym}/T. \quad (3)$$

An analogous relation is derived for β. The symmetry coefficient C_{sym} is directly related to the symmetry energy (per nucleon) of a given fragment having asymmetry I, $E_{sym} = C_{sym}I^2$. Isoscaling is not limited to models within the grand-canonical approximation. As a matter of fact, eq. (3) was first derived in the expanding emitting-source EES model [45,46]. Isoscaling predictions have also been observed in different statistical multifragmentation models [29].

There is an alternative explanation within the statistical multifragmentation model why isoscaling should appear in finite systems. In most SMMs, a variant of the liquid-drop mass formula is used. Charge distribution of fragments with fixed mass numbers A, as well as mass distributions for fixed Z, are approximately Gaussian with average values and variances which are connected with the T and C_{sym} [44]. With a Gaussian distribution for the charge Z, for instance, we obtain, for fragments with a given mass A: $Y(Z) = \exp(-(Z-\langle Z\rangle)^2/2\sigma_Z^2)$. The ratio of this observable for two different systems is given by

$$Y_2(Z)/Y_1(Z) = c\exp\Big(-\frac{Z^2}{2}(1/\sigma_2^2 - 1/\sigma_1^2) + Z(\langle Z\rangle_2/\sigma_2^2 - \langle Z\rangle_1/\sigma_1^2)\Big). \quad (4)$$

If the variances σ_1 and σ_2 are equal, then isoscaling is observed. This is not unlikely since, in the approximation $\sigma_Z \approx \sqrt{(AT/8C_{sym})}$, the variances depend only on the temperature and the symmetry-term coefficient. A similar

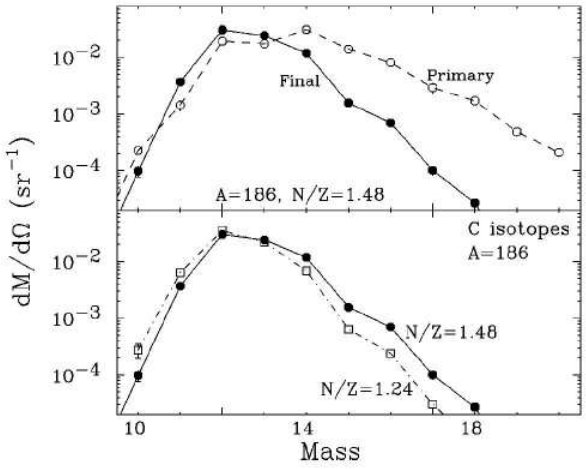

Fig. 10. Top: mass distribution of carbon isotopes, as obtained for the indicated systems, in SMM calculations, for primary hot fragments and final fragments. Bottom: predictions for final fragments are compared for two systems with different N/Z. From [46].

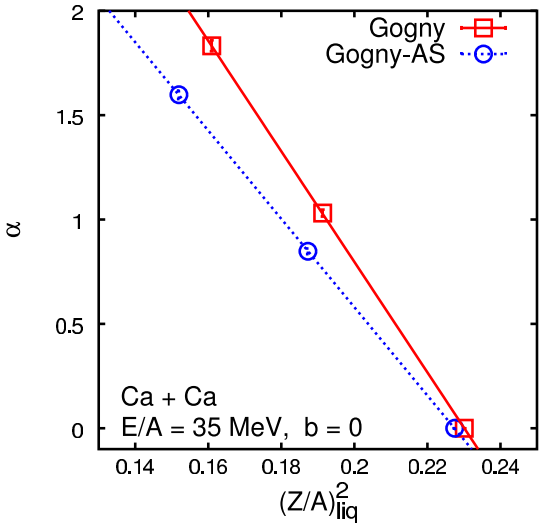

Fig. 11. Isoscaling parameter α, as a function of $(Z/A)^2_{liq}$ as obtained in AMD calculations with two different parameterizations of the symmetry energy.

expression for the mass distributions at given Z is also obtained [44].

In cases when the experimental masses are used, the isotope distributions are not strictly Gaussian. Figure 10 shows the hot carbon isotope distributions predicted by the canonical ISMM (open circles, top panel) from a source with $A_0 = 186, Z_0 = 75$ and $T = 5\,\mathrm{MeV}$, $\rho/\rho_0 = 1/6$. The solid circles correspond to the isotope distributions after sequential decays. Neither the primary nor the final distributions are Gaussian. Nonetheless, from two fragmenting sources with different (N_0/Z_0), one can derive the yield ratios and observe isoscaling [46]. In such calculations, isoscaling parameters are only slightly modified by the secondary-decay process, when the stable masses with the standard value of C_{sym} are used in the calculations. The effect of secondary decay is much larger if C_{sym} takes on lower values as will be discussed in sect. 4.4.2.

4.2 Origin of isoscaling in reaction dynamics

Isoscaling has been observed also in dynamical fragmentation models, such as the AMD model [18], QMD [47] and classical molecular dynamics (CMD) [19], as well as in SMF calculations [48] and in quasi-analytical calculations of the spinodal decomposition process [49]. For instance, fig. 11 shows the dependence of α on the charge to mass ratio, $(Z/A)^2_{liq}$, of the liquid phase for the collisions of Ca isotopes, at 35 MeV/A, as predicted by the AMD model. A linear dependence of α on $(Z/A)^2_{liq}$ is observed. The two lines correspond to two different symmetry potentials used in the simulations (full line, asy-soft, Gogny; dotted line, asy-stiff, Gogny-AS). Thus, even in dynamical models, isoscaling is intimately related to the symmetry energy.

The study of isoscaling through dynamical simulations can elucidate the origin of this phenomenon. If chemical equilibrium is reached during the fragmentation process, it is clear that one can apply the considerations outlined in the previous section and directly relate the isoscaling parameter to the value of the symmetry energy and the temperature.

However, the linear relation between α and $(Z/A)^2$ can be obtained in different conditions, without assuming statistical equilibrium. If the origin of fluctuations in a multi-fragmenting system can be considered a "white noise" source, then the probability to observe a given fluctuation of the isovector density $\delta\rho_i = \delta\rho_n - \delta\rho_p$, in a given volume V, can be expressed (for small amplitude fluctuations) as

$$P \approx \exp(-\delta\rho_i^2/2\sigma_{\rho_i}), \tag{5}$$

where the variance σ_{ρ_i} depends on the fragmentation mechanism. Then, for a fragment of volume V and mass A, the distribution $P(N-Z)$ can be written as

$$P(N-Z) \approx \exp(-[N-Z-(\bar{N}-\bar{Z})]^2/(\mathcal{F}\rho_{in}V)), \tag{6}$$

where $\bar{N}$ and $\bar{Z}$ are the average neutron and proton numbers in the volume V, and σ_{ρ_i} is proportional to ρ_{in}, the density of the fragmenting system [50]. $\mathcal{F}$ is a constant that depends on the symmetry energy and the temperature.

In spinodal decomposition, for instance, fragments are formed (and their density grows) due to the development of isoscalar-like unstable modes. Hence isoscalar density fluctuations grow while the isovector variance does not evolve and keeps the memory of the initial isovector fluctuations of the unstable diluted source. Therefore, we may expect reduced iso-vector fluctuations (and larger isoscaling parameters) with respect to the statistical case, where the isotopic content of the entire fragment mass may fluctuate.

As an example, the results of SMF, based on the spinodal decomposition scenario, are presented in fig. 12 [48].

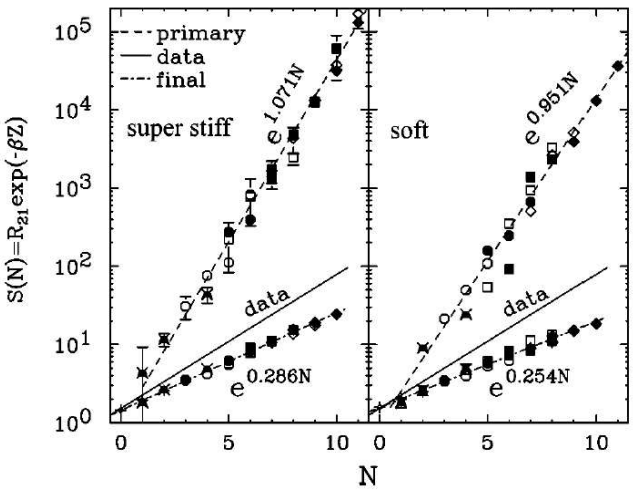

Fig. 12. Scaled isotope yield ratio, as a function of N, as obtained in SMF calculations of central reactions $^{124}\mathrm{Sn} + ^{124}\mathrm{Sn}$ and $^{112}\mathrm{Sn} + ^{112}\mathrm{Sn}$, at 50 MeV/A, for primary and final fragments. Two parameterizations of the symmetry energy are considered. From [48].

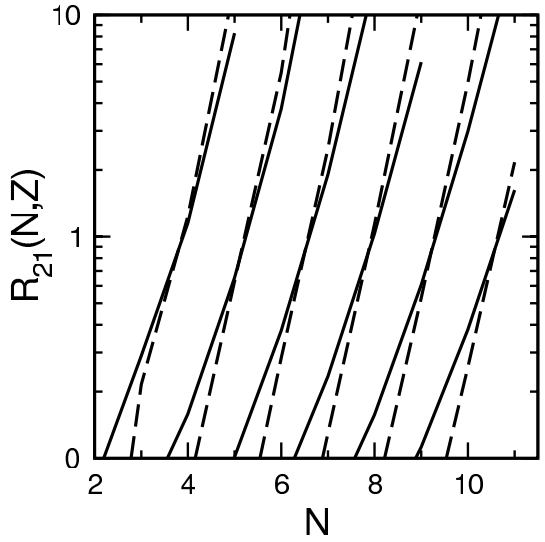

Fig. 13. Yield ratio $R_{21}(N,Z) = Y_{\alpha=0.2}(N,Z)/Y_{\alpha=0.1}(N,Z)$ calculated with the "super-stiff" symmetry term (solid lines) and with the asy-soft symmetry term (dashed lines). Lines correspond to different values of Z, Z = 3–8 from left to right. The system is prepared with density and temperature inside the spinodal region. The average values of the slope approximatively are 2.2 and 1.5 for the asy-soft case and the asy-super-stiff case, respectively. From [49].

Here large isoscaling parameters are observed for the primary fragments. However, they are significantly affected by the secondary decay and final values appear closer to the data. But the relative differences between the two parameterizations of the symmetry energy used are also much reduced.

The results obtained in a quasi-analytical description of spinodal decomposition, comparing fragment production in nuclear matter with asymmetry $I = 0.2$ and $I = 0.1$, are presented in fig. 13, for two parameterizations of the symmetry term [49].

The formula can be recast as follows:

$$P(Z,N) \approx \exp(-[(N-Z)^2/A - N(4(\bar{Z}/A)^2 - 1) - Z(4(\bar{N}/A)^2 - 1)]/[\mathcal{F}/\eta]), \quad (7)$$

where η is the ratio between the fragment final density $\rho_{fin} = A/V$ and the initial density ρ_{in} (η larger or equal to 1).

In statistical models η is equal to 1 and $\mathcal{F}$ coincides with T/C_{sym}, while in the early spinodal decomposition process the variance of the fragment isotopic distribution, due to isovector fluctuations, is reduced with respect to the equilibrium value $\mathcal{F}$. However it should be noted that, within such a scenario, isoscalar-like modes also contribute to the variance, due to the beating of several unstable modes, that bear a different distillation effect [49].

If one assumes that $\bar{Z}/A$ (and $\bar{N}/A$) depends only slightly on A and can be related to the average distillation effect, that determines the average asymmetry of the formed fragments, then from eq. (7) the isoscaling parameters are equal to

$$\alpha = 4((Z_1/A_1)^2 - (Z_2/A_2)^2)/(\mathcal{F}/\eta),$$
$$\beta = 4((N_1/A_1)^2 - (N_2/A_2)^2)/(\mathcal{F}/\eta). \quad (8)$$

Hence one gets the same formal expression as in statistical models, but with a more complex relation of the isoscaling parameters to the system properties. These parameters appear connected to the distillation effect, but also to the width of the isotopic distributions, that can in general differ from the predictions of statistical models.

The link between isoscaling parameters and symmetry energy depends on the way fragments are formed, while the observation of isoscaling and the relation to the $(Z/A)_{liq}$ value of the liquid phase appear as quite general properties and do not require the assumption of statistical equilibrium.

4.3 Temperature dependence of isoscaling

With the availability of models, we are able to explore the temperature dependence of isoscaling. All calculations (statistical or dynamical) show that the isoscaling parameters are inversely related to the temperature. So we would expect these parameters to decrease with increasing temperature, excitation energy or incident energy. Indeed, such phenomenon was observed in refs. [39,51]. Figure 14 shows the isoscaling parameter α as a function of the incident energy. In this study, isobars with mass $A = 58$ (^{58}Ni and ^{58}Fe) are used as target and projectile. Reaction 1 is taken to be the symmetric $^{58}\mathrm{Ni} + ^{58}\mathrm{Ni}$ which has the initial $(N/Z)_{ini}$ value of 1.07. For the upper curve (solid points), reaction 2 is taken to be the symmetric system $^{58}\mathrm{Fe} + ^{58}\mathrm{Fe}$ with $(N/Z)_{ini} = 1.23$ and, for the lower curve, the mixed system, $^{58}\mathrm{Fe} + ^{58}\mathrm{Ni}$, with $(N/Z)_{ini} = 1.15$ is used as reaction 2. This figure clearly shows that the α

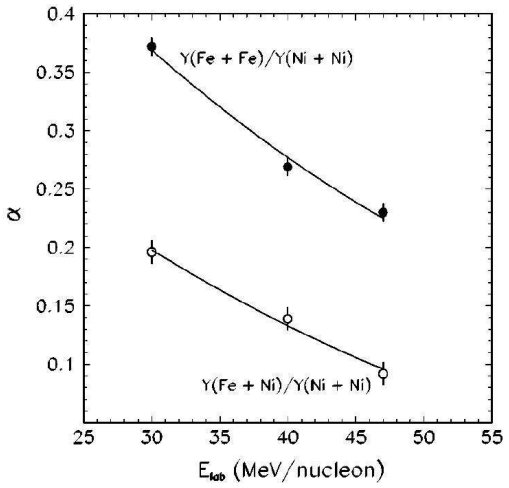

Fig. 14. Evolution of the isoscaling parameter α, as obtained in central collisions, *versus* the beam energy. From [52].

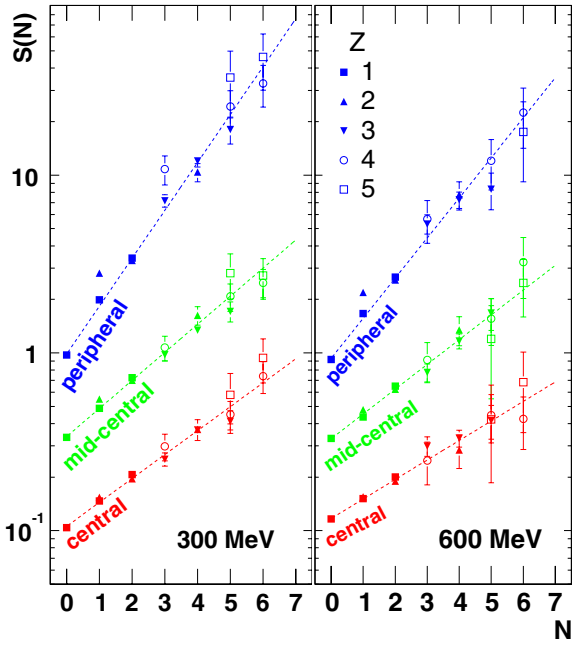

Fig. 15. Scaled isotopic ratios for $^{12}C + ^{112,124}Sn$ at 300 (left) and 600 (right) MeV/A. Three different centrality bins are considered. From [53].

value decreases with incident energy from $E/A = 30$ MeV to 47 MeV. In addition, there is also a clear drop in the α values with the decrease of the $(N/Z)_{ini}$ values of the entrance channel. The latter has also been observed in the collisions of central Sn isotopes which first established the phenomenon of isoscaling [30].

Isoscaling has been studied in fragmentation processes of excited target residues, in the reactions $^{12}C + ^{112,124}Sn$ at 300, 600 MeV/A [53]. Due to large uncertainties in the IMF isotope ratios, the isoscaling parameter α is mainly determined by the light charged particles, $Z = 1, 2$ (see fig. 15). The isoscaling parameter α is observed to decrease with increasing centrality of the reaction and the beam energy. Even though the temperature (measured from isotope ratios) increases with centrality, the density of the emitting source in the peripheral collisions is expected to be larger than the density of the fragment formation created in the central collisions. Thus this experiment does not offer solid proof that α decreases with increasing temperature.

4.4 Extraction of symmetry energy from isoscaling analysis

In the past few years, there have been many attempts to extract information on the density behaviour of the symmetry energy from the isoscaling analysis of fragmentation reactions [44,51–56]. In the following we will review recent developments in this field.

4.4.1 Insights from theoretical models

In the absence of equilibrium, the isoscaling parameter is not directly connected to the symmetry energy value. This is surely the case of SMF calculations, where large values of the isoscaling parameters are obtained for primary fragments, that do not reflect the low value of the symmetry energy observed in the model at the fragmentation stage.

If equilibrium is achieved as in statistical models, eq. (3) suggests that it is possible to extract information on the symmetry energy coefficient from the isoscaling analysis of the data. However, eq. (3) is strictly valid for primary fragments only. If experimental data are used, one must examine the effects of sequential decays on the variables α, $\Delta(Z/A)^2$, and T. To study the dependence of different parameters on the stiffness of the symmetry term in the nuclear EOS, it is useful to obtain some insights from model simulations.

The dependence of the α values as a function of stiffness parameters was first obtained in expanding emitting-source (EES) model calculation. In ref. [31], two sources with initial charge of 100 and initial mass of 224 for source 1 and 248 for source 2, initial thermal excitation energies of 9.5 MeV and collective radial expansion energies of 2.5 MeV (corresponding to the compound systems of $^{112}Sn + ^{112}Sn$ and $^{124}Sn + ^{124}Sn$ reactions at $E/A = 50$ MeV) are assumed in the calculations. In the model a power law dependence of $C_{sym} = 24.3(\rho/\rho_0)^\gamma$ is used to describe the fragmentation stage [31]. A nearly linear decrease of the isoscaling parameter α with γ is observed as shown in fig. 16. This suggests that the α value is larger for smaller γ, consistent with more neutrons emitted with an asy-soft interactions as discussed in sect. 3.

Unlike the EES and dynamical models, most statistical models assume that $C_{sym} (\approx 25$ MeV) is constant throughout the reaction. In most cases, this value is the same as the symmetry energy coefficient in the liquid-drop mass formula used in the model. Recently, the effects of the symmetry energy coefficient on fragment isotope distributions is studied with a microcanonical Markov-chain version of the statistical multifragmentation model [53]. The

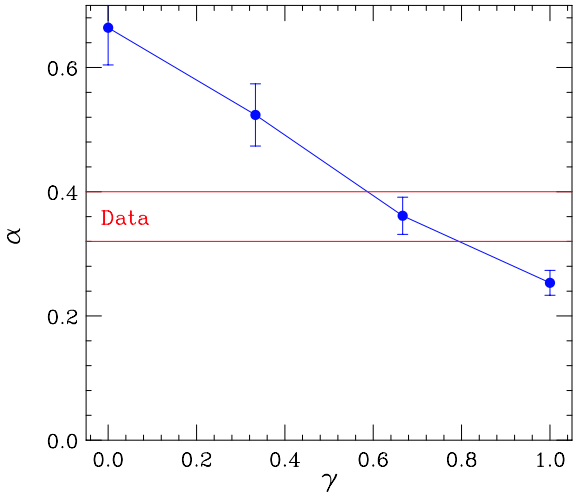

Fig. 16. Theoretical EES model predictions for the isoscaling parameter α extracted from the emitted $Z = 3$–6 fragments. From [31].

target nuclei ^{112,124}Sn with excitation energies of 4,6 and 8 MeV/A were chosen as inputs and the symmetry energy C_{sym} was varied between 4 and 25 MeV in the model. The isoscaling coefficient α was determined from the calculated fragment yields before (hot fragments) and after (cold fragments) the sequential decay stage of the calculations. The hot fragments exhibit the linear increase of α values with increase in C_{sym}. In the low-density region, larger symmetry energy corresponds to asy-soft interactions. Thus the trend is consistent with that observed in the EES calculations.

With $C_{sym} \approx 25$ MeV, the sequential processes lower the α values by 10% to 20% [29]. However, at small values of C_{sym}, one gets surprisingly the opposite effect: the decay of the wings of the wider distributions of hot fragments, which is directed towards the valley of stability, leads to larger isoscaling coefficients (see fig. 17). Thus, the effect of sequential decays on α not only depends on the excitation energy but also depends on C_{sym}.

To further examine the sensitivity of the isoscaling parameters to the different steps of the reaction (pre-equilibrium emission, fragmentation stage, secondary de-excitation), the three quantities in eq. (3), α, $\Delta(Z/A)^2$ and $\xi = \alpha/(4\Delta(Z/A)^2)$ obtained from the AMD simulations of the central collisions of Ca isotopes are shown in fig. 18. ^{40}Ca + ^{40}Ca is chosen as reaction 1 in eq. (1) [57]. Reaction 2 of ^{48}Ca + ^{48}Ca and that of ^{60}Ca + ^{60}Ca are labeled in the figure. From the figure one can see that the isoscaling parameters are affected by the isospin-dependent pre-equilibrium emission and distillation effects which change the Z_0/A_0 of the source, and by the symmetry energy during the fragmentation stage, that influences the width of the isotopic distribution through the value of ξ (see eq. (8)). One may also note the compensation between the two effects: while ξ is larger in the asy-soft case (Gogny, closed points), $\Delta(Z/A)^2$ is larger in the asy-stiff case (Gogny-AS, open points).

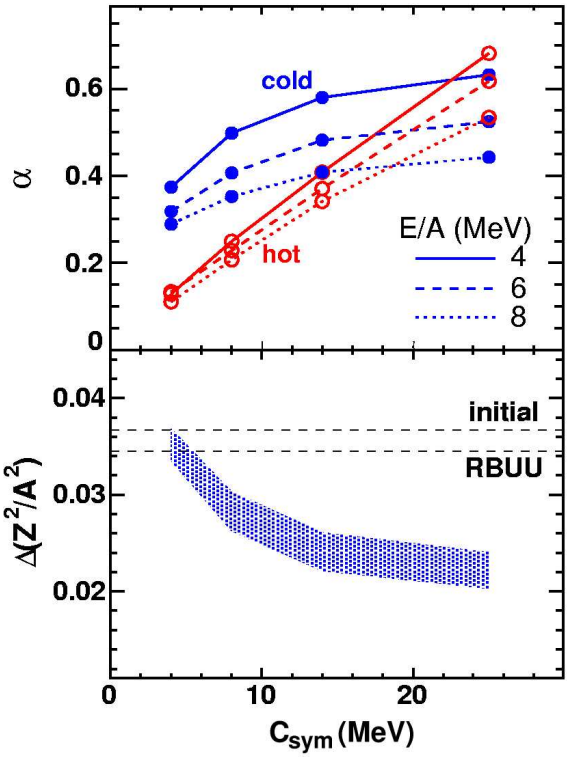

Fig. 17. The isoscaling parameter α, as obtained in SMM calculations for the same system as in fig. 15, as a function of the symmetry energy coefficient, for primary and final fragments. From [53].

As expected from isoscaling, α is nearly independent of the charge number of the isotopes. We note that while α (bottom panel), $\Delta(Z/A)^2$ (middle panel) depend on the reaction systems and the interacting potentials (Gogny (asy-soft, closed diamonds) and Gogny-AS (open squares)), $\xi = \alpha/(4\Delta(Z/A)^2)$ only depends on the interacting potentials. For asy-soft (Gogny) interaction, the symmetry energy is larger resulting in larger α and smaller $\Delta(Z/A)^2$ values (solid symbols) as compared to the corresponding values (open symbols) obtained if the asy-stiff (Gogny-AS) interaction is used. This trend is consistent with the results from the EES and SMM simulations.

To further examine the effects of sequential decays, the primary fragments emitted in the collisions of the Ca isotopes in AMD simulations are then allowed to decay and the corresponding quantities are plotted in fig. 19. Isoscaling is still preserved but the α values no longer show a difference between the two interactions. Furthermore, all the three quantities, α, $\Delta(Z/A)^2$ and ξ have very different values before and after sequential decays. To extract the correct information on the symmetry energy, ξ, (*i.e.* the value before decay), one must use the values of α and $\Delta(Z/A)^2$ from the primary fragments.

4.4.2 Experimental extraction of symmetry energy

One of the major objectives in heavy-ion collisions is to extract the density dependence of the symmetry energy

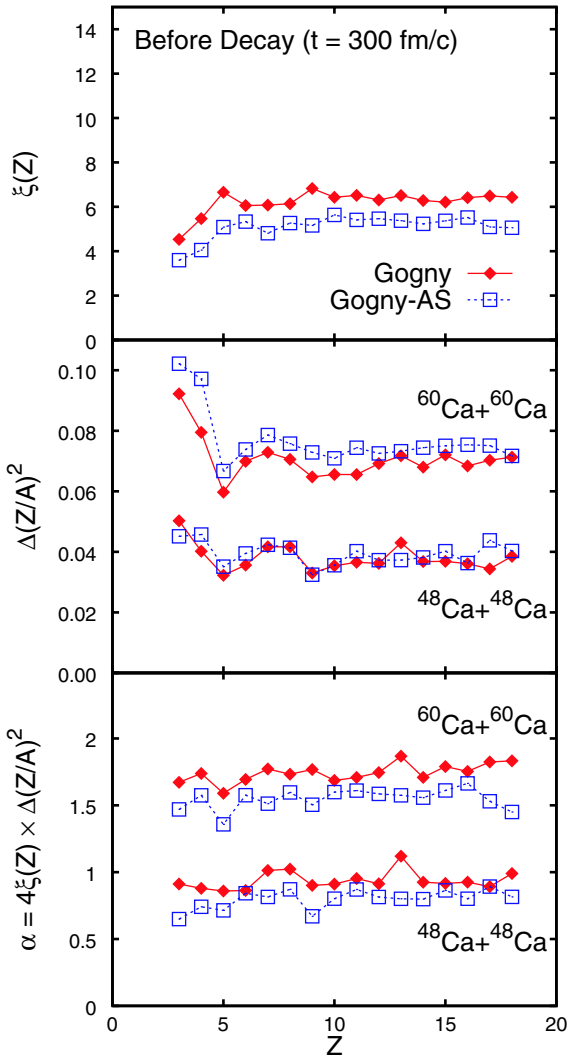

Fig. 18. The three quantities $\xi(Z)$ (top), $\Delta(Z/A)^2$ (middle) and α (bottom) for the primary fragments, as obtained in AMD calculations. The results with the Gogny and Gogny-AS forces are shown by filled diamonds and the open squares, respectively. From [57].

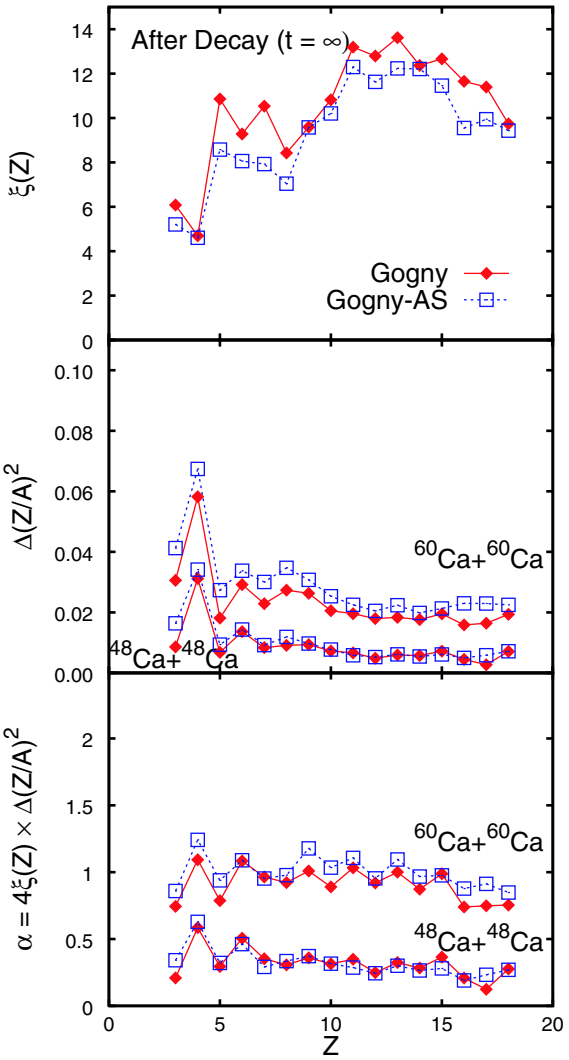

Fig. 19. The same as fig. 18 but for the final fragments. From [57].

in the nuclear equation of state. Since only ground-state particles are detected experimentally, theoretical models are needed to extrapolate the properties of the primary fragments or to simulate the effects of sequential decays. Unfortunately, theoretical developments in heavy-ion reactions have not reached the state that calculations can be done *a priori*. Nonetheless, we will review a few cases where isoscaling is used in the analysis.

In ref. [54], dynamical models are employed to deduce the $(Z/A)_{liq}$ of the liquid phase after pre-equilibrium emission, while the fragmentation stage is described by statistical models. Using this hybrid approach, it is concluded that an asy-stiff parameterization of C_{sym} leads to better agreement with the isoscaling analysis (^{112}Sn + ^{112}Sn and ^{124}Sn + ^{124}Sn at 50 MeV/A). The result, especially the trend, is in contradiction with the results from the same data analyzed with the expanding emitting-source model as shown in fig. 16. To understand the inconsistency, we examine the contributions of each stage of the calculations. The BUU stage predicts a larger $\Delta(Z/A)^2$ value with asy-super-stiff interaction, this is similar to the predictions of EES, SMM and AMD discussed in last section. Accordingly, it is expected that the SMM fragmentation and decay stage would predict a smaller alpha value. However, the results from the hybrid calculation are just the opposite. One explanation is that inconsistent results are obtained if the dynamical stage (when symmetry energy evolves with density and time) is coupled with a statistical stage (when a fixed value of $C_{sym} \approx 25$ MeV is adopted).

The dependence of the isoscaling parameter on the symmetry interaction, simulated by the AMD model [18] has been used to analyze several systems at $T \approx 3.5$ MeV [44,56], indicating that the data are more consistent with the Gogny-AS (asy-stiff) interaction, see fig. 20 [52]. To perform this comparison, an estimation of the $(Z/A)^2_{liq}$ is deduced, as a function of the $(Z/A)^2_{ini}$ of the initial system, by extrapolating the results of AMD

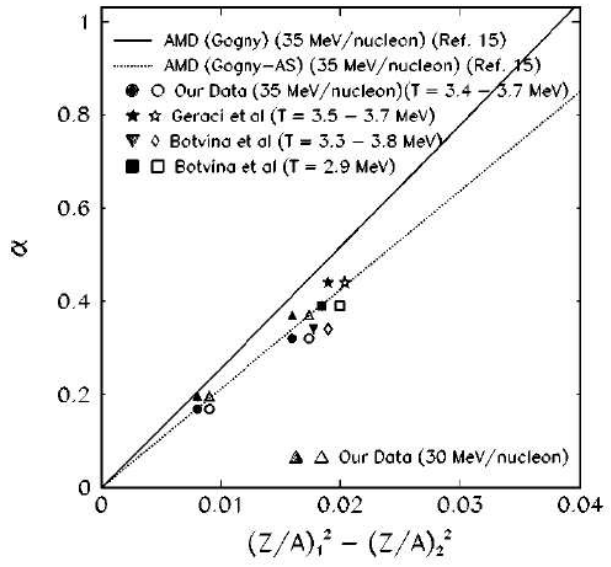

Fig. 20. Isoscaling parameter α, as a function of the difference $\Delta(Z/A)^2_{liq}$ between the two compared systems, as obtained in AMD calculations with two different parameterizations of the symmetry energy. The points refer to the isoscaling parameter extracted from several experimental data (see text for detail). From [52].

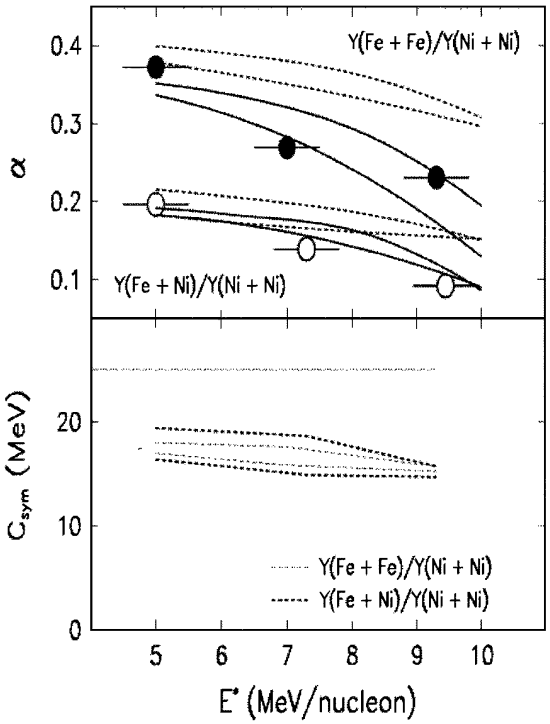

Fig. 21. Top: isoscaling parameter α *versus* the excitation energy, as obtained in the data (circles) and in SMM calculations for primary (dashed) or final (full lines) fragments. The band associated with calculations are due to uncertainty in the size of the fragmenting source. Bottom: symmetry energy coefficient, as extracted from α, assuming statistical equilibrium. From [51].

calculations for the Ca systems shown in fig. 11. Recent studies show that such extrapolations may not be valid outside the simulated range of impact parameters [58]. The isoscaling parameter deduced from the experimental data is compared with the results of the AMD model. However, this comparison is done without considering the secondary-decay effect which is large.

Other studies aimed to extract the symmetry energy value at the freeze-out configuration directly from the data assuming that thermal and chemical equilibrium have been reached. To do so, one needs to extract from the data the isoscaling parameter, as well as the temperature and the (Z_0/A_0) of the emitting source. In the study performed in ref. [51], the value of (Z_0/A_0), as provided by BNV calculations with a fixed value of C_{sym}, is used. The set of data has been analyzed with SMM calculations. The latter, that take into account the secondary decay, are in qualitatively good agreement with the experimental value of the isoscaling parameters. As it appears from the calculations, for a fixed value of the symmetry energy (around 25 MeV), the final isoscaling parameter, that can be compared to data, appears to be lower than the one obtained from the primary fragment yields, especially at high excitation energies. This observation is used to correct the experimental parameter, to try to remove the influence of the secondary de-excitation process. Then one can use eq. (3) to extract the value of the symmetry energy, once the temperature has been estimated. The results obtained for the symmetry energy are shown in fig. 21. Low symmetry energy values were obtained. However, it should be noted that the results of the analysis depend on the use of a hybrid model; the estimation of the (Z_0/A_0) of the emitting sources is determined by the BNV model and sequential decay effects are obtained from the SMM. As discussed before, such approach has its own problems.

A similar analysis is performed in ref. [53], where fragmentation processes of excited target residues produced in the reactions $^{12}C + ^{112,124}Sn$ at 300, 600 MeV/A are studied. The symmetry energy coefficient is extracted from the isoscaling parameters using eq. (3) and assuming that the Z_0/A_0 of the fragmenting sources is the same as the initial systems. The extracted C_{sym} value changes from 25 MeV to a value around 15 MeV (see fig. 22) when the centrality of the reaction is increased.

However, as stressed above, in this kind of analysis one has to use the isoscaling parameters as deduced from the primary fragments and not the final ones. So the authors try to go back to the properties of the primary fragments with the help of new SMM simulations, where the density dependence of the symmetry energy is partly taken into account by changing the symmetry energy constants used in the mass formula (see fig. 17).

This means that to get the observed isoscaling parameters for central reactions, C_{sym} should assume even lower values (4 MeV or less). These results would point to a strong reduction of the symmetry energy (and hence a strong dilution of the system) at the time of chemical freeze-out. It is clear, however, that any conclusion

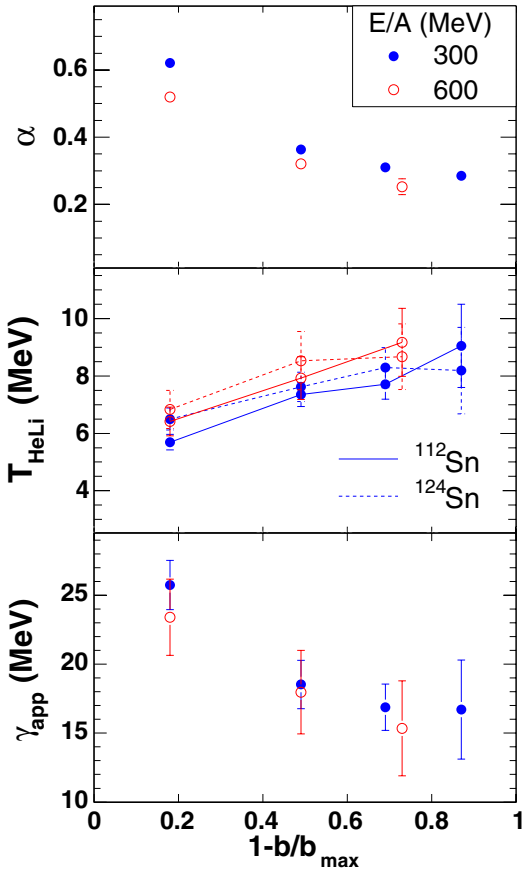

Fig. 22. Evolution of the isoscaling parameter *versus* the impact parameter, for the same reactions as in fig. 15 (top panel). The evolution of the temperature of the TLF sources and of the extracted apparent symmetry energy coefficient are shown in the middle and bottom panels, respectively. From [53].

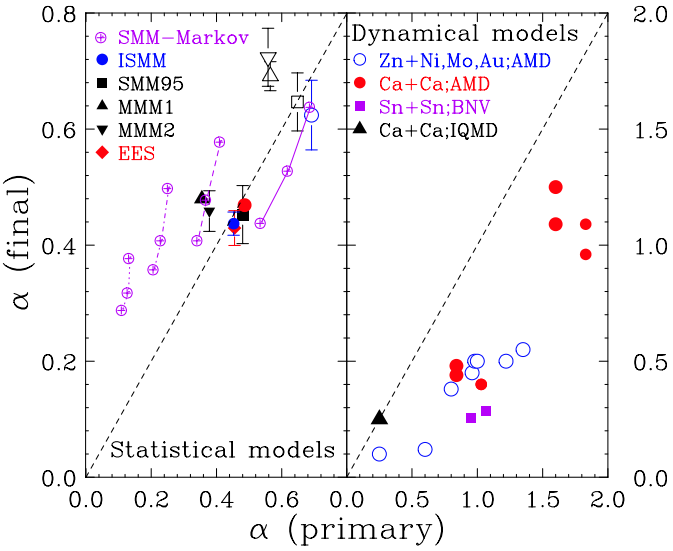

Fig. 23. Effect of sequential decays on the isoscaling parameter, α, for statistical models (left panel) and for dynamical models (right panel).

in this direction depends on the isotopic evolution of the multi-fragmenting system as it approaches the chemical freeze-out. Moreover, the results are only based on the predictions of the SMM and on a particular way to implement the density dependence of the symmetry energy in a fragmenting system.

While the effects of sequential decay on α and $\Delta(Z/A)^2$ and T are important in any analysis that involves using eq. (3) to extract the symmetry energy, such effects are not easy to evaluate and may depend on specific models. In fig. 23, we have compiled the α values before (horizontal axis) and after (vertical axis) sequential decays obtained for many systems using statistical models (left panel) and dynamical models (right panel). The statistical models used include statistical multifragmentaton models such as SMM95, I(mproved)SMM, microcanonical Markov-chain version of the SMM, microcanonical multifragmentation model (MMM), and the expanding emitting source (EES) [29]. The three dynamical models used are the asymmetrized molecular dynamical model, AMD, the Boltzmann-Nordheim-Vlasov model, BNV and the isospin quantum molecular dynamical models, IQMD. In general, the α values from primary fragments are much larger in dynamical models such as SMF (fig. 13) and AMD (figs. 18 and 19) models than statistical multifragmentation models. (Note the difference in the vertical scale of the left and right panel of fig. 23.) Sequential decay effects reduce the α values in nearly all dynamical models and the effects are large, more than 50%. Such large effects obscure the differences in the isoscaling parameters from realistic interactions (see fig. 19).

The trend is not as clear in statistical models. For $C_{sym} \approx 25$ MeV (including results from SMM-Markov chain calculations joined by the solid lines), the sequential decay effects are small. However, if lower C_{sym} values are used, as in the simulations shown in fig. 17 [53], the α values increase after sequential decays (points joined by dot-dashed, dashed and dotted lines). It is unphysical to assume a constant C_{sym} throughout the expansion phase when fragments are formed. Furthermore, when the C_{sym} values are reduced, there will be a mismatch of the masses of the excited fragments and the ground-state fragments. More study is needed to understand the sequential-decay effects in isoscaling.

In conclusion, isoscaling remains a nice algorithm in data analysis. Unfortunately, the extraction of the symmetry energy using eq. (3) is not so transparent due to the uncertainties in the determination of the (Z_0/A_0) of the emitting source and the secondary-decay effects on the isoscaling parameter α of the emitting source. Our current understanding of the sequential-decay effects on primary fragments is not adequate to allow us to distinguish different realistic asy-EOS interactions. On the positive side, all studies seem to support that much lower values of the symmetry energy than that of normal nuclei are obtained in the low-density region when multifragmentation occurs. This is also in agreement with the results of AMD simulations [18]. Ideally, one should study the properties of the primary fragments directly from experiments. Alter-

natively, one could find an observable which cancels out the effects of sequential decays as well as other undesirable effects from Coulomb repulsion and pre-equilibrium emissions. The latter two effects mimic the effects from symmetry energy. From the theoretical point of view, it is crucial to follow the whole reaction path within the same model, including the same density dependence of the symmetry term in the equation of state from start to finish. Hybrid models definitely have drawbacks and should be used with caution.

5 Isospin transport

In peripheral collisions it is possible to identify projectile-like and target-like residues in model calculations, as well as in experiments. Calculations suggest that at incident energy above 30 MeV per nucleon and for charge-asymmetric reactions, the symmetry term of the nuclear EOS provides a significant driving force that speeds up the isospin equilibration between the two reaction partners. Thus peripheral collisions may allow one to measure the time scales for charge and mass transport and diffusion. The degree of equilibration, correlated to the interaction time, should provide some insights into transport properties of fermionic systems and, in particular, give information on transport coefficients of asymmetric nuclear matter [59].

5.1 Insight into isospin transport in nuclear reactions

The mechanisms responsible for isospin transport can be essentially related to the presence of isospin, but also to density gradients along the reaction path. Isospin diffusion bears information about the value of the symmetry energy at low density, while the drift (transport in the presence of density gradients) is more connected to the derivative of the symmetry energy.

In asymmetric systems, isospin transport can arise from isospin gradients (diffusion) and from density gradients (drift). Through the low-density neck region, density gradients may be present also in binary systems. The neutron-excess is pushed towards the low-density regions, because this situation is energetically more favorable. This mechanism can induce isospin transport even in reactions between nuclei with the same N/Z [60].

The role of the EOS in isospin transport mechanisms can be made more explicit by studying the response of nuclear matter, in the presence of neutron and proton density gradients. Since we are mostly facing situations where local thermal equilibrium is reached, we will discuss results obtained within the hydrodynamic limit, where the derivation of the isospin transport coefficients is more transparent.

In such a framework the proton and neutron migration is dictated by the spatial gradients of the corresponding chemical potentials $\mu_{p/n}(\rho_p, \rho_n, T)$, where ρ_p and ρ_n are proton and neutron density and T denotes the temperature [10,61]. The currents of the two species can be expressed, in terms of the total density $\rho = \rho_n + \rho_p$ and asymmetry $I = (\rho_n - \rho_p)/\rho$, as follows:

$$j_n = D_n^\rho \nabla\rho - D_n^I \nabla I, \tag{9}$$

$$j_p = D_p^\rho \nabla\rho - D_p^I \nabla I, \tag{10}$$

where D_q^ρ and D_q^I are drift and diffusion coefficients due to density and isospin gradients, respectively:

$$D_q^\rho = ct \left(\frac{\partial \mu_q}{\partial \rho}\right)_{I,T}, \tag{11}$$

$$D_q^I = -ct \left(\frac{\partial \mu_q}{\partial I}\right)_{\rho,T}, \quad (q = n, p) \tag{12}$$

(ct is a negative constant).

They can be expressed as

$$D_q^\rho = ct\left[N^{-1} + \frac{\partial U}{\partial \rho} \pm 2I\frac{\partial C_{sym}}{\partial \rho} + O(I^2)\right], \tag{13}$$

$$D_q^I = \pm 2ct\ \rho\left[C_{sym} \pm I\left(\rho\frac{\partial C_{sym}}{\partial \rho} - C_{sym}\right)\right], \quad (+n, -p), \tag{14}$$

where N^{-1} is the level density of symmetric matter at the same density and temperature and $U(\rho)$ is the isoscalar part of the mean-field potential.

One can see that the isovector part of the nuclear interaction enters the coefficients D_q^ρ through the derivative of the total symmetry energy C_{sym}. On the other hand, the isospin diffusion coefficients D_q^I depend, in leading order, on C_{sym}. Moreover, it appears that the difference of neutron and proton drift coefficients, $D_n^\rho - D_p^\rho = \frac{\partial(\mu_n - \mu_p)}{\partial \rho}$, is equal to $4I\frac{\partial C_{sym}}{\partial \rho}$, as one can simply derive from the relation $\mu_n - \mu_p = 4C_{sym}I$.

In conclusion, the diffusion appears essentially related to the value of the symmetry energy, while the drift is connected to its derivative. From this study one can see more clearly that the isospin distillation effect, as discussed in sect. 3, which originates from the presence of density gradients in the fragmentation process, is sensitive essentially to the derivative of the symmetry energy at low density.

5.2 Experimental studies and comparison with calculations

Experimentally, one examines the isoscaling properties of the fragments originating from the (projectile) residues. Figure 24 shows the isoscaling phenomenon observed in the reaction of ^{124}Sn (projectile) + ^{112}Sn (target) and its inverse reaction ^{112}Sn (projectile) + ^{124}Sn (target) [16]. Unlike the central collision isoscaling data, the slope is larger for the reaction with neutron-rich projectile than the reaction with the proton-rich projectile. Differences in the asymmetric systems reflect the driving force that

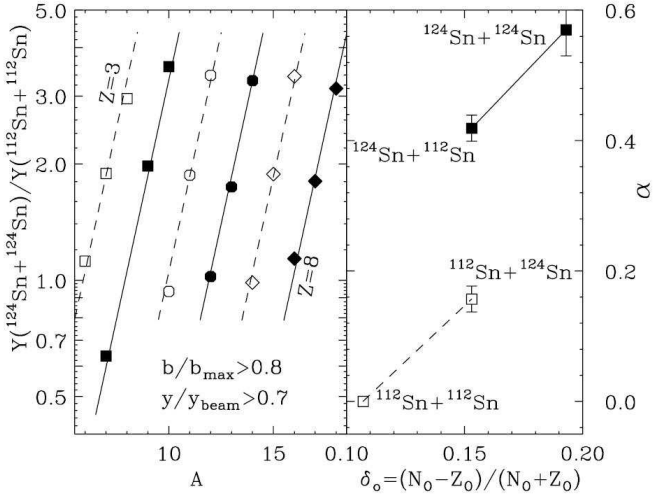

Fig. 24. Isotope yield ratios, as a function of the mass A, for fragments emitted from PLF in peripheral collisions (left). The isoscaling parameters, as obtained in different projectile-target combinations, are compared in the right part of the figure. From [16].

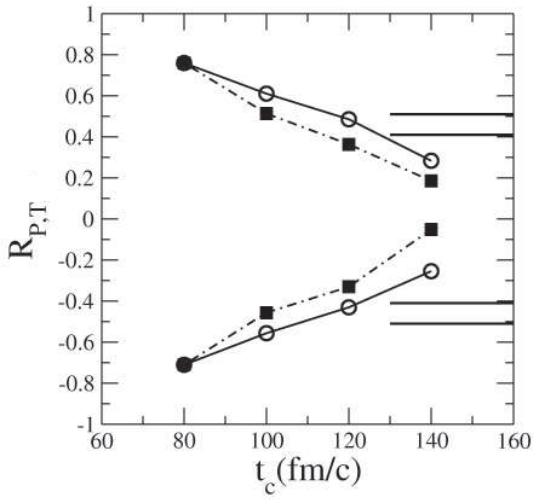

Fig. 25. The isospin transport ratio $R_{P,T}$, eq. (15), for the asy-soft (full squares) and asy-super-stiff (circles) interactions as a function of the interaction time t_c, corresponding to different impact parameter b, in the range 6–10 fm. The band between the two solid lines corresponds to the experimental data of [16].

causes isospin diffusion. As shown before, the force arises from the symmetry term in the equation of state. If the force is weak, one would not expect any isospin mixing to occur and the α value should resemble those of the projectiles in the symmetric systems. In order to quantify the transition from no isospin diffusion to complete mixing, the isospin transport ratio, R_i is used

$$R_i = \frac{2O_{PT} - O_{PP} - O_{TT}}{O_{PP} - O_{TT}}\,. \qquad (15)$$

Here $P, (T)$ stands for the projectile-like (target-like) fragment. The quantities O_i refer, in general, to any isospin-dependent observable, characterizing the fragments at separation time, for the mixed reaction (PT, ^{124}Sn + ^{112}Sn or ^{112}Sn + ^{124}Sn), the reactions between the neutron-rich (PP, ^{124}Sn + ^{124}Sn), and between the neutron-poor nuclei (TT, ^{112}Sn + ^{112}Sn), respectively. Similar ratios constructed using free protons have been used as isospin tracer in central heavy-ion collisions [62], to check stopping and thermal equilibration. The insensitivity to systematic errors and the ability to calibrate the observables from the two symmetric systems, ^{124}Sn + ^{124}Sn and ^{112}Sn + ^{112}Sn to +1 and −1 offer many advantages. It has been shown that non-isospin effects such as effects from Coulomb force will be largely canceled using the isospin transport ratio [63]. Furthermore, in comparison with calculations that cannot predict the same experimental observables, due to model limitations, one can use another observable to construct the isospin transport ratios as long as both the experimental and theoretical observables are linearly related to each other. For example, in model calculations, one can use the asymmetry $I = (N - Z)/A$ of the emitting source, instead of isoscaling, to evaluate the transport (imbalance) ratio since, to the first order, α and I are linearly related. In fact, as we have seen previously, α, as extracted from primary fragments, is related to the difference $(\frac{Z_1^2}{A_1^2} - \frac{Z_2^2}{A_2^2})$, which for not too large asymmetries can be rewritten as $(I_2 - I_1)/2$. The linear relation between α and I has been confirmed experimentally [30,56], suggesting that it holds for the isoscaling parameters extracted from the final fragments. Hence, the asymmetry of projectile-like or target-like residues can be used as the observable O in eq. (15).

The dependence of isospin transport (and equilibration) on the centrality of the reaction has been investigated in ref. [64] using SMF simulations without momentum dependence. Figure 25 shows the isospin transport ratio as a function of the interaction time t_c among the two reaction partners, that is inversely related to the impact parameter, for two interactions: an asy-super-stiff (open symbols) and an asy-soft (SKM*) (solid symbols) interactions. A more detailed analysis shows that it is possible to explicitly estimate the effects of isospin transport and pre-equilibrium emission on the transport ratios R. The interplay between the two processes leads to a stronger equilibration for asy-soft EOS, as it is evidenced by the isospin transport ratio. Actually, in the asy-super-stiff case, a larger isospin transfer is observed in the calculations, due to the presence of density gradients, directed from PLF and TLF towards the neck region, in line with the analytical predictions illustrated above. Indeed, in the asy-stiff case, the derivative of the symmetry energy, just below normal density, acquires larger values. However, we observe a kind of compensation between the asymmetry of the matter transferred from projectile to target (I_{PT}) and from target to projectile(I_{TP}), so finally isospin equilibration is more effective in the asy-soft case.

In refs. [16,65] BUU calculations which use different density dependence of the symmetry terms in the equation of state are performed for the same system at $b = 6$ fm. In

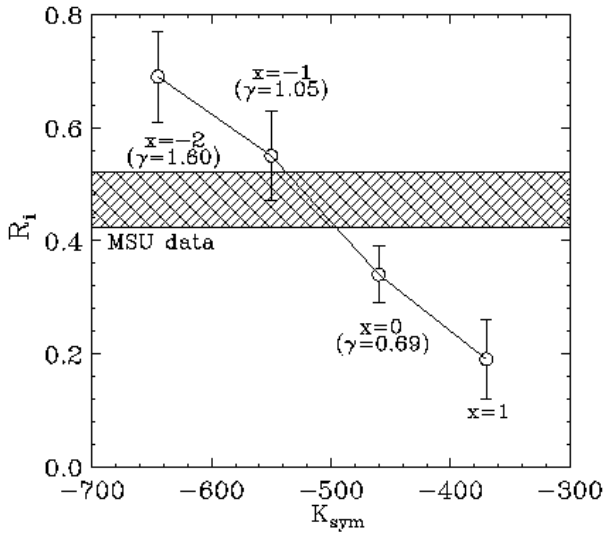

Fig. 26. Isospin transport ratio, relative to peripheral collisions of ^{124}Sn + ^{112}Sn, $E/A = 50$ MeV, as obtained in the data (hatched area) and in model calculations using different parameterizations of the symmetry energy.

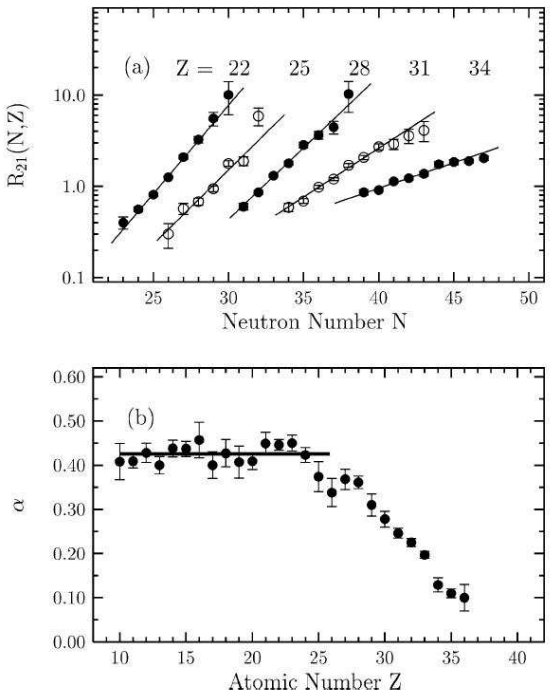

Fig. 27. a) Yield ratios $R_{21}(N,Z)$ of projectile residues from the reactions ^{86}Kr + ^{112,124}Sn at 25 MeV/A, with respect to N, for the Z's indicated. b) Isoscaling parameter α *versus* the charge of the fragment Z. The straight line is a constant value fit for the lighter fragments $Z = 10$–26. From [55].

fig. 26, the parameter x indicates the stiffness of the symmetry term, ranging from an asy-soft behaviour (larger x) to an asy-stiff behaviour (negative x). Momentum dependence is included in the calculations. Within error bars, the isospin transport ratio R_i decreases with the softness of the symmetry term suggesting that the driving force for isospin equilibration is much larger for the asy-soft interaction. Using the isoscaling fitting parameter α as the experimental isospin observable O in eq. (15), the isospin transport ratios of the two asymmetric systems shown in the right panel of fig. 24 appear as the two horizontal lines in fig. 25 and as the shaded region in fig. 26. Assuming that data can be directly compared with calculations performed at $b = 6$ fm, the best agreement is obtained in the range $x = -1, 0$. Without including momentum dependence in the calculations, a stiffer symmetry term would be needed to fit the data (see fig. 25 at 140 fm/c and [16]). This is due to the fact that the overall dynamics becomes more repulsive when the momentum dependence is included and isospin equilibration depends not only on the strength of the symmetry term, but also on the system interacting time.

It should be noted that this comparison is well suited only if one assumes that PLF and TLF fragments are near normal density, independent of the parameterization adopted for the symmetry energy. Otherwise, the isoscaling parameter cannot be simply related only to the (N_0/Z_0) of the source, but would also depend on the value of the symmetry energy, that is model dependent. It would be interesting to check this hypothesis using a model that includes fragmentation (such as AMD), and calculating the isospin transport ratio directly from the isotope yields, as done in the experiments. In this way one would better test the sensitivity of the results to the behaviour of the symmetry energy. In other words, as discussed in sect. 4.4, it is essential to consider the density dependence of the symmetry energy in the fragmentation process.

The dependence of the $(N/Z)_{PLF}$ *versus* the excitation energy of the system has been studied for the INDRA reactions, Ni + Ni and Ni + Au at 52 and 74 MeV/A [66], looking at the reconstructed PLF, in binary collisions. In the symmetric case, $(N/Z)_{PLF}$ is seen to increase with centrality due to a proton-rich pre-equilibrium emission. For the Ni + Au case, it is possible to observe isospin equilibration among the reaction partners.

In the analysis presented in ref. [55], the goal was to extract the $(N/Z)_{PLF}$ of the PLF sources and hence to discuss isospin equilibration between projectile and target. The systems ^{86}Kr + ^{112,124}Sn at 25 MeV/A have been considered (fig. 27). The isoscaling parameter α, as a function of the charge Z of the projectile residue, exhibits a plateau, at $Z \leq 22$. This would suggest that fragments are emitted from equilibrated sources formed in more central collisions. (Any source characterization will require impact parameter selection, not available in this data set.) As Z increases, a decrease of α is observed, *i.e.* the strict isoscaling relation of eq. (1) is not obeyed suggesting a non-equilibrium process. One interpretation of this observation is that the heavier fragments coming from PLFs are formed in more peripheral reactions. In the extreme case when the fragment composition is close to that of the projectile with little transfer of nucleons from the targets, $\Delta(Z/A)^2$ becomes small resulting in small α values.

6 Conclusions and outlook

From the results discussed above, several indications on the density dependence of the symmetry potential can be extracted from the study of reactions with charge-asymmetric systems in the Fermi energy domain. The isotopic content of emitted light particles and IMFs, as well as the reconstructed degree of N/Z equilibration between reaction partners, bear important information on the symmetry energy. We summarize below the main conclusions, as well as improvements and new studies that can be envisaged.

- In model calculations, the isotopic content of pre-equilibrium emission appears quite sensitive to the stiffness of the symmetry term, and to its momentum dependence. A more neutron-rich pre-equilibrium emission is expected for higher values of the symmetry energy. Thus experiments to measure the ratios of free neutrons and free protons will complement the results obtained with fragments. In fragment formation the degree of isospin fractionation (*i.e.* the transfer of the neutron excess towards the gas phase) is sensitive to the slope of the symmetry energy at low density.
- The isoscaling analysis, based on the comparison of the isotopic content of fragments emitted from systems with different initial asymmetries could in principle be used to extract the value of the symmetry energy in situations where equilibrium is reached. However, it is not so easy to disentangle the predictions given by the different parameterizations. Indeed not only the isoscaling parameters reflect the width of the isotopic distributions, but they are quite sensitive to the difference $\Delta(Z/A)^2$ between the fragments asymmetries of the two compared systems, that is also largely influenced by the symmetry energy behaviour. Hence, compensation effects diminish the sensitivity of the final results to the asy-EOS. Moreover, as shown by both statistical and dynamical simulations, large secondary decays may reduce significantly the differences coming from different symmetry terms in the EOS used in the models. However, most experimental results seem to suggest that the symmetry energy of excited fragments at low density may be lower than the symmetry energy at normal nuclear-matter density. However, the extraction of the accurate value of symmetry energy and the differentiation of different interactions require theoretical models to simulate the sequential-decay effects and the reaction path. More work is needed in model development. Experiments that can extract the properties of primary fragments directly will also advance our understanding in this issue.
- It would be important to perform a cross-check of model predictions against several experimental observables, sensitive to the different phases of a reaction, from pre-equilibrium emission to fragmentation and de-excitation stage. This allows better identification of the isotopic content of the gas and liquid phases, that is essential for the analysis of the de-excitation process of the excited primary products and related observables (such as isoscaling). The use of models that can follow the whole path of the reaction is highly desirable. This would also allow to ascertain the fragmentation mechanism and the way the system approaches chemical freeze-out. The study of correlations between the fragment isotopic content and kinematical properties can be envisaged as a tool to learn about time scales for fragment formation and N/Z equilibration.
- In semi-peripheral collisions, it is interesting to compare the behaviour of reactions with different entrance channel asymmetries to investigate isospin exchange between projectile and target. Indeed the N/Z equilibration among the reaction partners gives information about the strength of the symmetry term. However, it should be noticed that the amount of isospin exchange is also strictly connected to the interaction time, when the two reaction partners are in contact. This is clearly influenced also by the isoscalar part of the nuclear interaction. Hence, the sensitivity of this observable to the value of the symmetry energy is not so transparent. The study of the interplay between isoscalar and isovector parts of the nuclear interaction in the reaction dynamics deserves further attention.

MBT acknowledges the support of the National Science Foundation under Grant No. PHY-01-10253.

References

1. It is important to put the properties of *neutron* matter at *subnuclear* densities on as firm a footing as possible, not only for astrophysical applications, but also for interpreting terrestrial experiments with coming radioactive beam facilities", C.J. Pethick, D.G. Ravenhall, in *The Lives of Neutron Stars*, NATO ASI Ser. C **450**, 59 (1995).
2. I. Bombaci, T.T.S. Kuo, U. Lombardo, Phys. Rep. **242**, 165 (1994); I. Bombaci, Phys. Rev. C **55**, 1587 (1997).
3. M. Prakash *et al.*, Phys. Rep. **280**, 1 (1997).
4. I.M. Irvine, *Neutron Stars* (Oxford University Press, 1978).
5. J.M. Lattimer *et al.*, Phys. Rev. Lett. **66**, 2701 (1991).
6. D. Pines, R. Tamagaki, S. Tsuruta, *Neutron Stars* (Addison-Wesley, New York, 1992).
7. K. Sumiyashi, H. Toki, Astrophys. J. **422**, 700 (1994).
8. C.J. Pethick, D.G. Ravenhall, *The Lives of Neutron Stars*, NATO ASI Ser. C **450**, 59 (1995).
9. C.H. Lee, Phys. Rep. **275**, 255 (1996).
10. V. Baran, M. Colonna, V. Greco, M. Di Toro, Phys. Rep. **410**, 335 (2005).
11. H. Müller, B.D. Serot, Phys. Rev. C **52**, 2072 (1995).
12. Bao-An Li, C.M. Ko, Nucl. Phys. A **618**, 498 (1997).
13. M. Colonna, M. Di Toro, A. Larionov, Phys. Lett. B **428**, 1 (1998).
14. V. Baran, M. Colonna, M. Di Toro, V. Greco, Phys. Rev. Lett. **86**, 4492 (2001).
15. M. Colonna, Ph. Chomaz, S. Ayik, Phys. Rev. Lett. **88**, 122701 (2002).
16. M.B. Tsang, T.X. Liu, L. Shi *et al.*, Phys. Rev. Lett. **92**, 062701 (2004).

17. P. Sapienza *et al.*, Phys. Rev. Lett. **87**, 072701 (2001) and references therein.
18. A. Ono, P. Danielewicz, W.A. Friedman *et al.*, Phys. Rev. C **68**, 051601(R) (2003); Phys. Rev. C **70**, 041604 (2004).
19. C.O. Dorso *et al.*, arXiv: nucl-th/0504036.
20. W.P. Tan, S.R. Souza, R.J. Charity *et al.*, Phys. Rev. C **68**, 034609 (2003).
21. B-A Li, C.B. Das, S. Das Gupta *et al.*, Nucl. Phys. A **735**, 563 (2004).
22. J. Rizzo *et al.*, Nucl. Phys. A **732**, 202 (2004).
23. J.Y. Liu, W.J. Guo, Y.Z. Xing *et al.*, High En. Phys. Nucl. **29**, 456 (2005).
24. J. Rizzo, M. Colonna, M. Di Toro, arXiv: nucl-th/0508008.
25. J. Margueron, Ph. Chomaz, Phys. Rev. C **67**, 041602 (2003).
26. V. Baran *et al.*, Nucl. Phys. A **703**, 603 (2002).
27. S. Das Gupta, A.Z. Mekjian, M.B. Tsang, Adv. Nucl. Phys. **26**, 91 (2001).
28. C.B. Das, S. Das Gupta, W.G. Lynch, A.Z. Mekjian, M.B. Tsang, Phys. Rep. **406**, 1 (2005).
29. M.B. Tsang *et al.*, this topical issue.
30. H.S. Xu *et al.*, Phys. Rev. Lett. **85**, 716 (2000).
31. M.B. Tsang, W.A. Friedman, C.K. Gelbke *et al.*, Phys. Rev. Lett. **86**, 5023 (2001).
32. M. Veselsky, R.W. Ibbotson, R. Laforest *et al.*, Phys. Rev. C **62**, 041605 (2000).
33. J. Randrup, Nucl. Phys. A **307**, 319 (1978).
34. G.J. Kunde *et al.*, Phys. Rev. Lett. **77**, 2897 (1996).
35. M.L. Miller *et al.*, Phys. Rev. Lett. **82**, 1399 (1999).
36. Ph. Chomaz, F. Gulminelli, Phys. Lett. B **447**, 221 (1999).
37. P. Milazzo *et al.*, Phys. Rev. C **62**, 041602 (2000).
38. M.B. Tsang *et al.*, Phys. Rev. C **64**, 041603 (2001).
39. D.V. Shetty, S.J. Yennello, E. Martin *et al.*, Phys. Rev. C **68**, 021602 (2003).
40. G.A. Souliotis, M. Veselsky, D.V. Shetty *et al.*, Nucl. Phys. A **746**, 526c (2004).
41. M.N. Andronenko, L.N. Andronenko, W. Neubert, Prog. Theor. Phys. Suppl. **146**, 538 (2002).
42. M. Veselsky, G.A. Souliotis, M. Jandel, Phys. Rev. C **69**, 044607 (2004).
43. W.A. Friedman, Phys. Rev. C **69**, 031601 (2004).
44. A.S. Botvina, O.V. Lozhkin, W. Trautmann, Phys. Rev. C **65**, 044610 (2002).
45. W.A. Friedman, Phys. Rev. C **42**, 667 (1990).
46. M.B. Tsang *et al.*, Phys. Rev. C **64**, 054615 (2001).
47. Qingfeng Li, Zhuxia Li, Horst Stöcker, Phys. Rev. C **73**, 051601 (2006).
48. T.X. Liu, M.J. van Goethem, X.D. Liu *et al.*, Phys. Rev. C **69**, 014603 (2004).
49. M. Colonna, F. Matera, Phys. Rev. C **71**, 064605 (2005).
50. M. Colonna *et al.*, Phys. Rev. C **47**, 1395 (1993).
51. D.V. Shetty, A.S. Botvina, S.J. Yennello *et al.*, Phys. Rev. C **71**, 024602 (2005); D.V. Shetty, A.S. Botvina, S.J. Yennello *et al.*, Phys. Rev. C **71**, 029903(E) (2005).
52. D.V. Shetty, S.J. Yennello, A.S. Botvina *et al.*, Phys. Rev. C **70**, 011601 (2004).
53. A. Le Fèvre, G. Auger, M.L. Begemann-Blaich *et al.*, Phys. Rev. Lett. **94**, 162701 (2005).
54. W.P. Tan, B.-A. Li, R. Donangelo *et al.*, Phys. Rev. C **64**, 051901 (2001).
55. G.A. Souliotis, M. Veselsky, D. Shetty *et al.*, Phys. Lett. B **588**, 35 (2004).
56. E. Geraci *et al.*, Nucl. Phys. A **732**, 173 (2004).
57. A. Ono *et al.*, *Proceedings for VI Latin American Symposium on Nuclear Physics and Applications, Iguazu, Argentina (2005)*, to be published in Acta Phys. Hung. A.
58. A. Ono *et al.*, arXiv: nucl-ex/0507018.
59. L. Shi, P. Danielewicz, Phys. Rev. C **68**, 064604 (2003).
60. R. Lionti, V. Baran, M. Colonna, M. Di Toro, Phys. Lett. B **625**, 33 (2005).
61. R. Balian, *From Microphysics to Macrophysics*, Vol **II** (Springer Verlag, Berlin, 1992).
62. F. Rami *et al.*, Phys. Rev. Lett. **84**, 1120 (2000).
63. M.B. Tsang, T.X. Liu, W.G. Lynch, in *Proceedings of the International Workshop on Multifragmentation IWM2005, Catania, Italy, 2005*, edited by R. Bougault *et al.*, Conf. Proc. Vol. **91** (Italian Physical Society, Bologna, 2006) p. 123.
64. V. Baran, M. Colonna, M. Di Toro *et al.*, Phys. Rev. C **72**, 064620 (2005) arXiv: nucl-th/0506078,
65. L.-W. Chen, C.-M. Ko, B.-A. Li, Phys. Rev. Lett. **94**, 032701 (2005).
66. E. Galichet *et al.*, submitted to Nucl. Phys. A.